

chiral unit. Depending on the chemical functions involved, we found that sterics, electrostatic repulsions, and hydrogen bonds may contribute to a strong handedness bias. Metadynamics simulations were carried out on already described systems, as well as on the new ones for which an experimental validation of the prediction was subsequently implemented, leading to the design of a proline-based chiral building block compatible with the solid phase synthesis of these oligoamides and their use in water.

Oligoamides of 8-amino-2-quinolinecarboxylic acid have been extensively demonstrated to adopt stable helical conformations in a wide range of solvents (Figure 1).^[12] The conformations

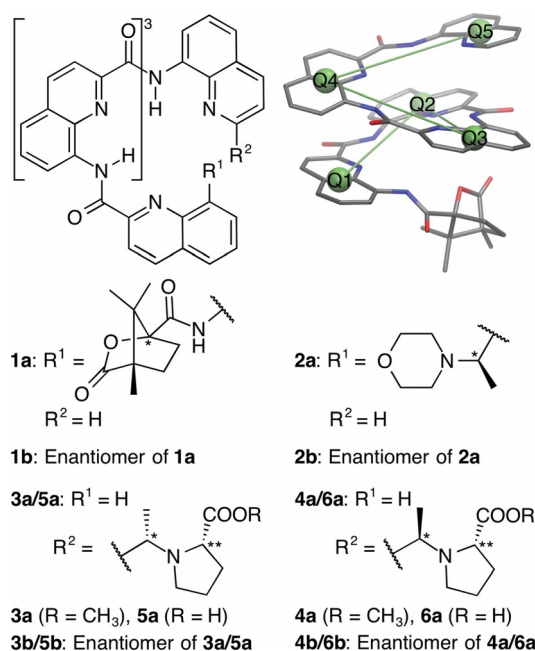


Figure 1. Structures of quinoline-carboxamide-based arylamide pentamers **1–6** with chiral, handedness biasing groups attached at either the N or C terminus. Top-right: example of a helically folded structure with the definition of the quinoline rings Q1 to Q5 and pitch dihedral angles. Stereogenic centers are marked with * and **.

mational stability in chloroform is considerable, with half-lives of handedness inversion ranging from minutes for short oligomers to days or weeks for longer ones.^[3b] Yet, even with these slow kinetics, handedness inversion does take place. The mechanism of helix reversal was recently demonstrated to consist of the propagation of an inversion center along the helix through the simultaneous unfolding and folding of two adjacent aryl–aryl linkages.^[3a] This conclusion was drawn from a metadynamics study, an approach^[13] that enables a complete description of the free energy landscape related to the handedness inversion of these oligomers despite the considerable energy barriers and the associated characteristic times that are well beyond the reach of classical molecular dynamics simulations.

Oligoquinoline carboxamide helical foldamers can be equipped with a variety of proteinogenic side chains that diverge from the helices. Depending on the resulting sequence,

selective interactions may occur with nucleic acids^[14] or with proteins.^[7a,15] Interactions were shown to be diastereoselective. They depend on the helix sense of the foldamer. Conversely, foldamer helix sense bias by a protein or a nucleic acid can actually be used as a method to detect interactions with biopolymers. There is thus great interest in controlling helical handedness of these oligomers. In an earlier study,^[4b] we reported that camphanylation of the N-terminal amine quantitatively (as far as NMR spectroscopy can detect) controls handedness. An oligomer such as **1a** (Figure 1), which bears a (1*R*)-(+)-camphanyl group, should be exclusively *M* helical. In search of a less bulky and less hydrophobic group, we subsequently described a quinoline unit bearing a morpholine-based stereogenic center at the N terminus that also effectively induces handedness.^[16] Oligomer **2a** with *R* chirality should be exclusively left-handed as well. However, at the start of this study, we had no group at our disposal to induce handedness effectively from the C terminus, a feature that would be useful since the N terminus would remain free to introduce other functionalities such as fluorescent dyes or protein ligands. Indeed, earlier attempts only yielded moderately effective C-terminal handedness inducers.^[17]

For this purpose, instead of undertaking potentially labor intensive experimental screening of numerous chiral groups at the C terminus, we endeavored in the development of a computational approach that would have a predictive value. In a first step, known oligomers **1a/1b** and **2a/2b** were studied using metadynamics to assess the accuracy of this method at predicting handedness bias. In a second step, new oligomers **3a/3b**, **4a/4b**, **5a/5b** and **6a/6b** which bear stereogenic centers at the C terminus, were also investigated, first computationally and then experimentally, and shown to be effective at handedness induction. The principles that guided the design of these oligomers included synthetic feasibility and the notion that stereogenic centers should be as close as possible to the main chain.

An important aspect of this work is that both computational and experimental studies were carried out in chloroform whereas the final use of these molecules is meant to be in water. This is because helix stability in water is so large^[12b,16] that handedness inversion does not occur anymore—helicity is kinetically inert at 25 °C for octamers or longer oligomers. Thus, helix handedness bias per se may not occur in water. To obtain a *P* or *M* helix in water one has to let a handedness-inducing group operate in a solvent such as chloroform, where helicity is dynamic, and then dissolve the helically biased structure in water where it does not change anymore.

Our results show the predictive value of metadynamics in this case. Calculations allow the prediction of whether a helix handedness bias occurs under the influence of the chiral group. These calculations also reveal the interactions (sterics, electrostatics, hydrogen bonds) responsible for a particular helix sense preference. Beyond their immediate applicability to oligoquinoline carboxamide helices, this approach potentially bears significance for the numerous other helical aromatic oligomers in which some handedness preference was demonstrated.^[18]

Results and Discussion

The metadynamics free-energy molecular dynamics method^[13] with force field parameters specifically optimized for the quinoline-carboxamide-based arylamides^[19] was applied to investigate helix handedness inversion and bias of pentameric oligomers 1–6 in chloroform (explicit solvent). Computations were systematically carried out on each enantiomer to assess their reproducibility. From these simulations, we determined the free-energy profiles (FEPs) of handedness inversion pathways with respect to two collective variables (CVs). The CVs are two pitch dihedral angles, Q1-Q2-Q3-Q4 and Q2-Q3-Q4-Q5 (Figure 1, top right), defined by the centers of masses (COMs) of four consecutive aromatic rings. Their sign identifies the handedness of the helix: positive for *P* and negative for *M* helices. Computational set-up details are described in our previous study of the helix handedness inversion.^[3a]

Helix handedness bias in camphanylated oligomers 1a/1b

Metadynamics studies of the previously described camphanylated pentamers 1a and 1b indicated a helix sense preference consistent with experiments,^[4b] as well as with each other. The FEP of 1a, which possesses an (*R*)-camphanyl group, yields an *M* helix as the global minimum and a *P* helix about 4 kcal mol⁻¹ higher in free energy (Figure 2b). In the FEP of enantiomer 1b, the *P* helix was found to be more stable by ≈ 3 kcal mol⁻¹ (Figure S1, Supporting Information). The difference between 3 and 4 kcal mol⁻¹ indicates an error margin associated with conformational sampling, yet both numbers are consistent with the > 99% biasing observed experimentally.^[4b]

A comparative analysis of the structural features of the lower energy (*M*)-1a/(*P*)-1b and the higher energy (*P*)-1a/(*M*)-1b was conducted by extracting conformations from the *M*- and *P*-helical basins using the 400 ns metadynamics trajectories. Structural characteristics of the extracted (*P*)-1b conformations agree well with the crystal structure of a corresponding *P*

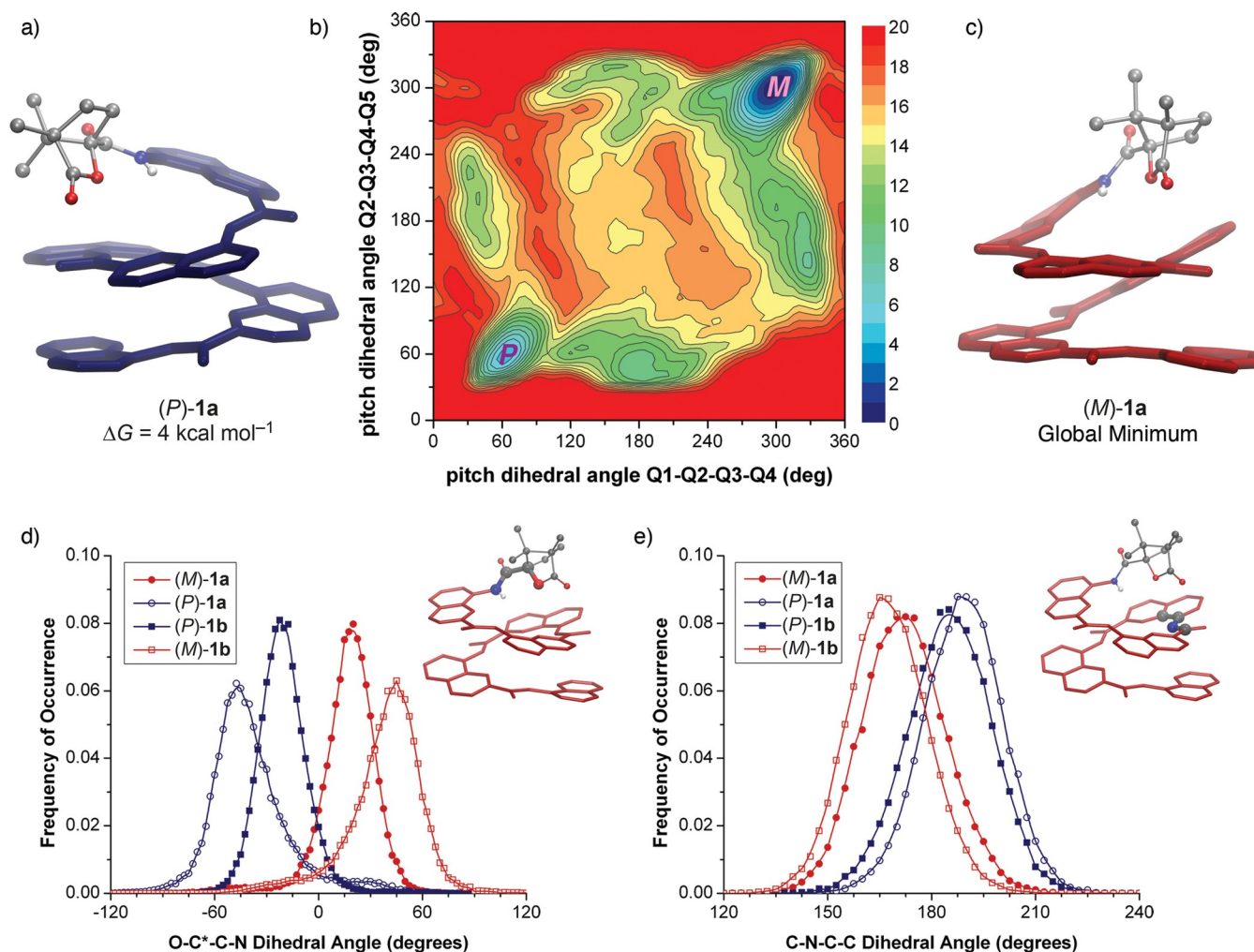


Figure 2. Free-energy profile (b, energy in kcal mol⁻¹) with respect to the two pitch dihedral angles of 1a in chloroform. Snapshots (c, a) of the conformations from the two helical basins (*M*)-1a and (*P*)-1a. Distributions (d, e) of backbone atomistic dihedral angles of the (*M*)-1a/(*P*)-1b and (*P*)-1a/(*M*)-1b conformations. Dihedral angles are displayed in the upper-right corner of each respective distribution.

helical (*S*)-camphanyl trimer,^[4b] despite the different conditions of the two, that is, solution versus solid environment and dynamic versus static structures. Both feature 2.5 units per turn and a helical pitch of around 3.5 to 3.6 Å. In addition, the (*P*)-**1b** conformational ensemble gives, for example, a normal distribution for the O-C*-C-N dihedral angle (Figure 2d) that peaks at -20° with a standard deviation (s.d.) of 11.6°. It thus encloses the crystal value of -15°. Similarly, the Q1-Q3 distance MD distribution peaks at 4.8 (s.d. 0.5) Å, and is 4.3 Å in the crystal structure; the Q1-Q2-Q3 angle peaks at 38° (s.d. 4.0°) in MD distribution, and is 36° in the crystal structure. The major difference between the preferred and non-preferred conformations was observed in the distribution of the O-C*-C-N dihedral angle which reflects the orientation of the camphanyl group with respect to the helix (insert, Figure 2d). This angle peaks at ±20° for (*M*)-**1a**/*(P)*-**1b**, and at ±50° for (*P*)-**1a**/*(M)*-**1b**. In the former, the closer-to-planarity distribution is driven by an N-H...O intramolecular hydrogen bond between the camphanyl endocyclic oxygen atom and the amide N-H. This H-bond is lost in the less favored (*P*)-**1a**/*(M)*-**1b** in which rotation around the central C*-C bond of the O-C*-C-N dihedral pushes the camphanyl group away from the helix center in order to minimize the steric clash between the backbone Q3 unit and a methyl group on the camphanyl moiety (position 7). This rotation lengthens the (N)H...O distance, thus diminishing the energetically favorable hydrogen-bonding interaction. In addition, in the less favored (*P*)-**1a**/*(M)*-**1b**, backbone aryl-amide bonds between Q2 and Q3 also rotate away from planarity to help distance the Q3 unit from the camphanyl methyl group (Figure 2e). This deviation stretches the helix, thus loosening aromatic contacts and weakening intramolecular hydrogen bonds between the amide NH and the aromatic endocyclic nitrogen atoms. Dissection of molecular mechanics (MM) energy into internal (bond, bend and torsion), electrostatic (e.g., hydrogen bonding) and van der Waals (e.g., sterics) components shows that, on average, the preferred (*M*)-**1a**/*(P)*-**1b** conformations have lower energy than the non-preferred (*P*)-**1a**/*(M)*-**1b** in all three categories (Supporting Information). Thus, the (*R*)-camphanyl group favors *M* handedness because this combination allows a favorable arrangement of the camphanyl group with respect to the helix, that is, that the two methyl groups in position 7 point upward and away from the helix while a hydrogen bond is established. The other combination [(*R*)-camphanyl with *P* helix] forces the molecule to undergo various conformational changes to minimize the clash between the helix backbone and one of the two methyl groups which is now pointing downward and towards the backbone. The relatively large biasing (≈3–4 kcal mol⁻¹) comes from the loss of hydrogen bonding and aromatic stacking as well as from the increase in steric repulsion.

Helix handedness bias in morpholine-functionalized oligomers **2a/2b**

Same as the camphanyl case, the metadynamics FEPs of morpholine-functionalized **2a** (Figure 3a) and **2b** (Figure S2, Supporting Information) are consistent with each other. Calcula-

tions predict higher stability for (*M*)-**2a**/*(P)*-**2b** in agreement with experimental observations.^[16] However, the computationally obtained 0.6–0.8 kcal mol⁻¹ free-energy difference, roughly corresponding to a 75:25 bias, is slightly lower than the experimentally determined bias of about 97:3.^[20] Analysis of the structural and energetic features shows that both the preferred (*M*)-**2a**/*(P)*-**2b** and non-preferred (*P*)-**2a**/*(M)*-**2b** basins consist of multiple conformations (Figure 3b) due to rotations around two bonds: 1) the C*-C bond, connecting C* with the backbone quinoline position 8 (Figure 3c, insert), and 2) the N-C* bond, linking the morpholine nitrogen atom to C* (Figure 3e, insert). The rotation around the C*-C bond (Figure 3c) determines the relative positions of the three C* substituents of different bulkiness (Figure 3b, green spheres) with respect to the helix backbone. For (*M*)-**2a**/*(P)*-**2b**, the corresponding N-C*-C-C torsional angle has a single-peak distribution (Figure 3c) that reflects the optimal arrangement of the three substituents: the largest group (morpholine) is away from the helix, the mid-sized group (methyl) aligns itself with the helix backbone, and the smallest substituent (hydrogen) points towards the helix. Within this optimal general arrangement, (*M*)-**2a**/*(P)*-**2b** display conformational variations with respect to the rotation of the N-C* bond (Figure 3e). The distribution has two major peaks, at ≈60° [(*M'*)-**2a**] and ≈180° [(*M''*)-**2a**], and one minor peak at ≈300° (i.e., -60°). The corresponding (*P'*)-**2b** and (*P''*)-**2b** conformations (∠C-N-C*-C ≈ -60°, that is, 300°, and ≈180°, respectively) are mirror images of their (*M*)-**2a** counterparts. It should be noted that percent occurrence (reflected by the area under each peak) of the multiple conformations of (*M*)-**2a** is consistent with that of (*P*)-**2b**, with reasonable conformational sampling variations between the two simulations (**2a** vs. **2b**).

For the non-preferred (*P*)-**2a**/*(M)*-**2b** minima, conformational variations are seen in the N-C*-C-C torsion (Figure 3c), resulting in two different arrangements of the three substituents. However, neither of the arrangements [(*P1*)-**2a** and (*P2*)-**2a**, Figure 3b] is as suitable as those in (*M*)-**2a** due to the mismatch of the C* chirality and handedness of the helix. The largest substituent (morpholine) is now much closer to the helix backbone; additionally, in (*P2*)-**2a**, the mid-sized methyl group is pointing directly towards the helix. There are notable differences in helix backbone conformations between the preferred (*M*)-**2a**/*(P)*-**2b** and non-preferred (*P*)-**2a**/*(M)*-**2b** basins (Figures 3d,f). A large deviation in the Q1-Q2-Q3 curvature angle indicates that a part of the helix opens up to accommodate the substituent (either morpholine or methyl) that is aligning with or pointing towards the helix. Dissection of MM energy analogous to the camphanyl case shows again that, on average, the preferred (*M*)-**2a**/*(P)*-**2b** conformations have lower energy than non-preferred (*P*)-**2a**/*(M)*-**2b** ones in all three categories. In addition, the occurrence of the multiple conformations within one basin is due to the tradeoff of energy components. For example, (*P1*)-**2a** has higher van der Waals repulsion and reasonably stabilizing electrostatic interactions, whereas the situation is the opposite for (*P2*)-**2a** (higher electrostatic and lower van der Waals energies). In summary, unlike for **1a/1b**, the handedness bias in **2a/2b** appears to be driven by sterics alone: it is the right combination of chirality and handedness that allows

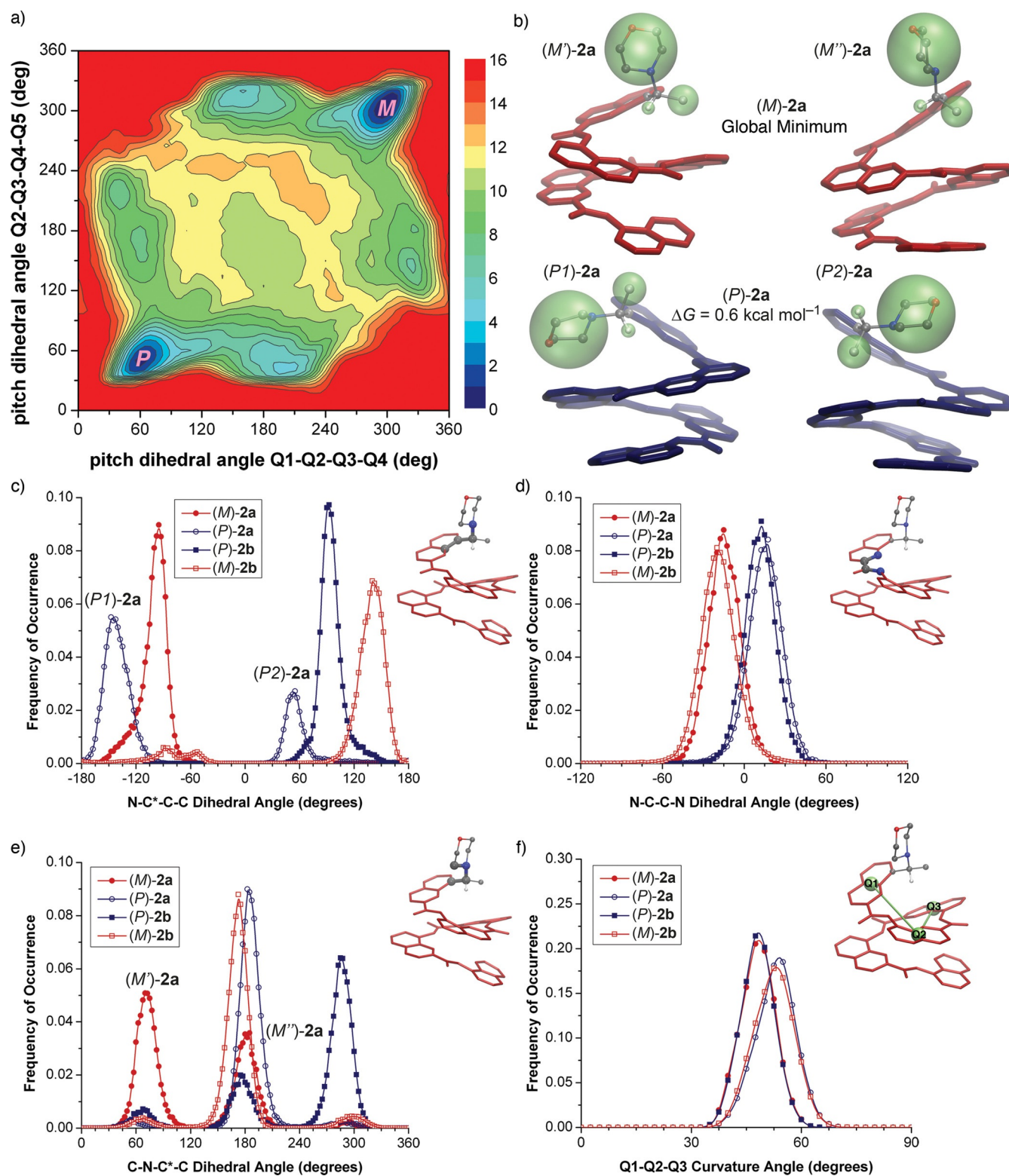


Figure 3. Free energy profile (a, energy in kcal mol⁻¹) with respect to the two pitch dihedral angles of 2a in chloroform. Snapshots (b) of the conformations from the two helical basins (M)-2a and (P)-2a. Distributions (c–e) of backbone atomistic dihedral angles of the (M)-2a/(P)-2b and (P)-2a/(M)-2b conformations. Distribution (f) of the Q1-Q2-Q3 curvature angle of the (M)-2a/(P)-2b and (P)-2a/(M)-2b conformations. The dihedral angles and curvature angle in question are displayed in the upper-right corner of each respective distribution.

sterically favorable arrangements of the C* substituents with respect to the helix.

Computational investigation of helix handedness bias in proline-functionalized oligomers **3a/3b** and **4a/4b**

In compounds **3a** to **6b**, a proline group is connected to the C-terminal quinoline (Q5) by a stereogenic (C*) center. In addition, a second stereogenic (C**) is naturally present within the proline group. These compounds had not been synthesized at the start of the computational studies. Their design followed the same simple principle as the design of **2a/2b**,^[16] that is, that a stereogenic center has a higher chance to promote helix handedness bias if it is placed close to the aromatic backbone. In the case of compounds **3a** to **6b**, the stereogenic center is located at the C terminus of the helix, thus leaving the N terminus available for further functionalization at the end of solid phase oligomer synthesis.^[7a,15] To consider both the acid and the methyl ester forms of proline, we carried out metadynamics simulations for four pairs of enantiomers: **3a/3b** and **4a/4b** are the *SS/RR* and *RS/SR* enantiomers in the methyl ester form, respectively; **5a/5b** and **6a/6b** are their acid form counterparts.

We find that the predicted biasing preferences are consistently opposite for **a** and **b** for all **a/b** pairs of enantiomers. Furthermore, the predicted bias for ester-terminated oligomers is of the same direction, but slightly weaker, than for the corresponding acid forms. Finally, chirality at C* alone, that is, the chiral carbon closer to the oligomer backbone, determines the biasing sense regardless of the configuration of the proline stereogenic center. Specifically, *S* C* chirality (**3a**, **4b**, **5a**, **6b**) promotes *P* helicity, whereas *R* C* chirality (**3b**, **4a**, **5b**, **6a**) promotes *M* helicity. In the following, we discuss **3a/3b** and **4a/4b** (results for **5a/5b** and **6a/6b** are available in the Supporting Information).

Similar to **2a/2b**, structural analysis of the proline-functionalized oligomers focuses on two rotatable bonds: 1) the C–C* bond, connecting the Q5 quinoline ring to the C* stereogenic center (Figure 4c, N–C–C*–N torsion); and 2) the C*–N bond, connecting the C* stereogenic center to proline (Figure 4e, C–C*–N–C** torsion). For the preferred (*P*)-**3a**/*(M)*-**3b** conformational basins, the N–C–C*–N dihedral angle distribution has a single peak at 90°/–90°, respectively. This again corresponds to the optimal arrangement of the three C* substituents according to their size, with the bulkiest group (proline) away from the helix, the midsized group (methyl) aligned with helix backbone and the smallest substituent (H) pointing towards the helix. Conformational variations within the (*P*)-**3a**/*(M)*-**3b** basin stem from the rotation of the C*–N bond, similarly to the rotation of morpholine mentioned above.

Conformational distributions of enantiomers were compared to assess the quality of conformational sampling. The C–C*–N–C** dihedral angle distribution peaks of (*P*)-**3a** and (*M*)-**3b** are symmetric with respect to 180° in both their size and positions (Figure 4e), indicating a sufficient level of conformational sampling in both cases. Conformational sampling differs somewhat for the non-preferred (*M*)-**3a**/*(P)*-**3b** pair. For (*M*)-**3a**, a single

conformation [(*M1*)-**3a**, Figure 4b], with $\chi_{\text{N-C-C*}-\text{N}} \approx 90^\circ$ and $\chi_{\text{C-C*}-\text{N-C**}} \approx -60^\circ$, dominates. In the case of its enantiomer (*P*)-**3b**, multiple conformations are found and the one that is mirror image of (*M1*)-**3a** [(*P1'*)-**3b** with $\chi_{\text{N-CC*}-\text{N}} \approx -90^\circ$ and $\chi_{\text{CC*}-\text{N-C**}} \approx 60^\circ$] accounts for 25% of all the (*P*)-**3b** conformations. Despite the difference in the conformational sampling, the free-energy difference (3.6 kcal mol⁻¹) between (*P*)-**3a** and (*M*)-**3a** is very similar to that (3.0 kcal mol⁻¹) between (*M*)-**3b** and (*P*)-**3b**. Energy decomposition shows that, on average, (*M*)-**3a** has unfavorable torsional and van der Waals energy, whereas (*P*)-**3b** has higher electrostatic energy. The larger difference in conformational sampling between the **3a** and **3b** enantiomers is in line with the fact that the proline substituent intrinsically has more degrees of freedom (more rotatable bonds, higher possibility of ring puckering) than, for example, the morpholine substituent. Therefore, the results from the paired simulations not only provide means for assessing the efficiency of sampling, but can also be used to access conformational space sampled in one, but not the other enantiomer simulation.

The effect of a mismatched C* chirality and helix handedness on the backbone conformation is more pronounced for **3a/3b** than for **2a/2b**. Both the CNCC backbone dihedral angle (Figure 4d) and the Q3–Q4–Q5 curvature angle (Figure 4f) in the non-preferred diastereomers open up to a larger extent in **3a/3b** than in **2a/2b** to accommodate the bulkier proline group. Thus, the helix stretches significantly more in the non-preferred (*M*)-**3a**/*(P)*-**3b** isomers than in the preferred (*P*)-**3a**/*(M)*-**3b**; this effect is stronger in **3a/3b** than in **2a/2b**.

Results for **4a/4b** are mostly in line with those of **3a/3b**, that is, **4a** has the same C* chirality as **3b**, and therefore shows a bias towards the *M* helix. However, due to the difference in the C** chirality between **4a** and **3b**, or **4b** and **3a**, there are a few notable differences. The first is the distribution of the N–C–C*–N dihedral angle (Figure 5c), which now features one major peak at $\approx -90^\circ/90^\circ$ [(*M2*)-**4a**/*(P2)*-**4b**], as well as minor peaks at $\approx (70^\circ/135^\circ)/-75^\circ$ [(*M1*)-**4a**/*(P1)*-**4b**] for the preferred (*M*)-**4a**/*(P)*-**4b** pair. This can be explained by examining the structures of (*M2'*)-**4a** and (*M2''*)-**4a** (Figure 5b). In both structures, the largest group, proline, is above the helix (optimal arrangement); however, the flip of the C** chirality now places the ester group either right on top of Q5 [(*M2'*)-**4a**], or pointing towards the helix [(*M2''*)-**4a**]. The destabilization caused by the added steric interaction allows the molecule to populate other conformational states such as (*M1''*)-**4a** or (*P1''*)-**4b**. Another difference is in the distribution of helix backbone torsional angle (Figure 4d) and helix curvature angle Q3–Q4–Q5. In the **4a/4b** series, both helix stretching and curvature opening are also observed. Although it seems that the difference of these distributions between the preferred (*M*)-**4a**/*(P)*-**4b** and non-preferred (*P*)-**4a**/*(M)*-**4b** is smaller than those from the **3a/3b** series, this is actually due to the shifts in peak positions of the preferred (*M*)-**4a**/*(P)*-**4b** groups. Therefore, the extent of helix backbone distortion for the non-preferred (*P*)-**4a**/*(M)*-**4b** group is similar to that of the (*M*)-**3a**/*(P)*-**3b** conformations, whereas the preferred (*M*)-**4a**/*(P)*-**4b** groups also distorted slightly away from those of (*P*)-**3a**/*(M)*-**3b**. Conforma-

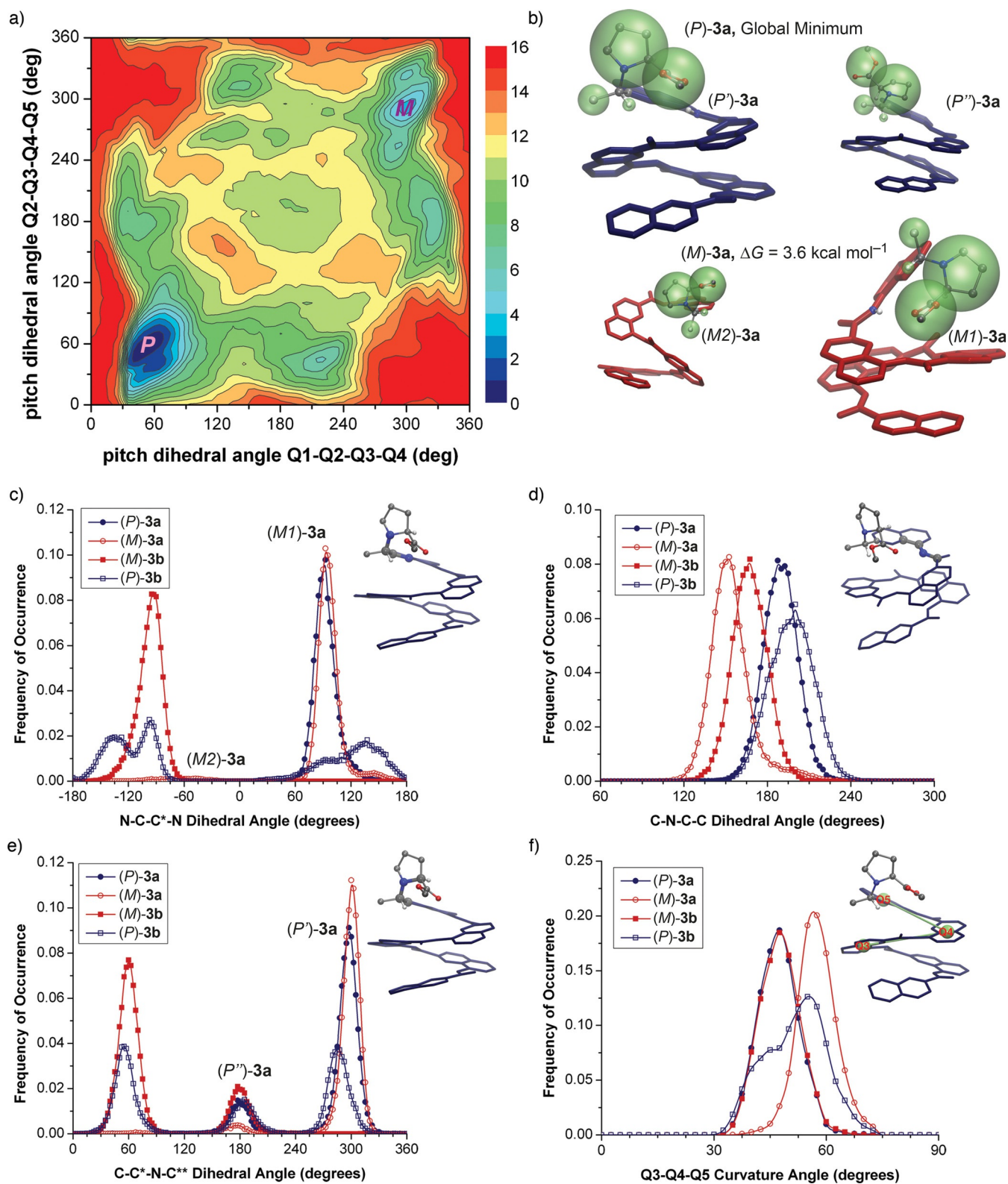


Figure 4. Free energy profile (a, energy in kcal mol⁻¹) with respect to the two pitch dihedral angles of **3a** in chloroform. Snapshots (b) of the conformations from the two helical basins (*P*)-**3a** and (*M*)-**3a**. Distributions (c–e) of backbone atomistic dihedral angles of the (*P*)-**3a**/*(M)*-**3b** and (*M*)-**3a**/*(P)*-**3b** conformations. Distribution (f) of the Q3-Q4-Q5 curvature angle of the (*P*)-**3a**/*(M)*-**3b** and (*M*)-**3a**/*(P)*-**3b** conformations. The dihedral angles and curvature angle in question are displayed in the upper-right corner of each respective distribution.

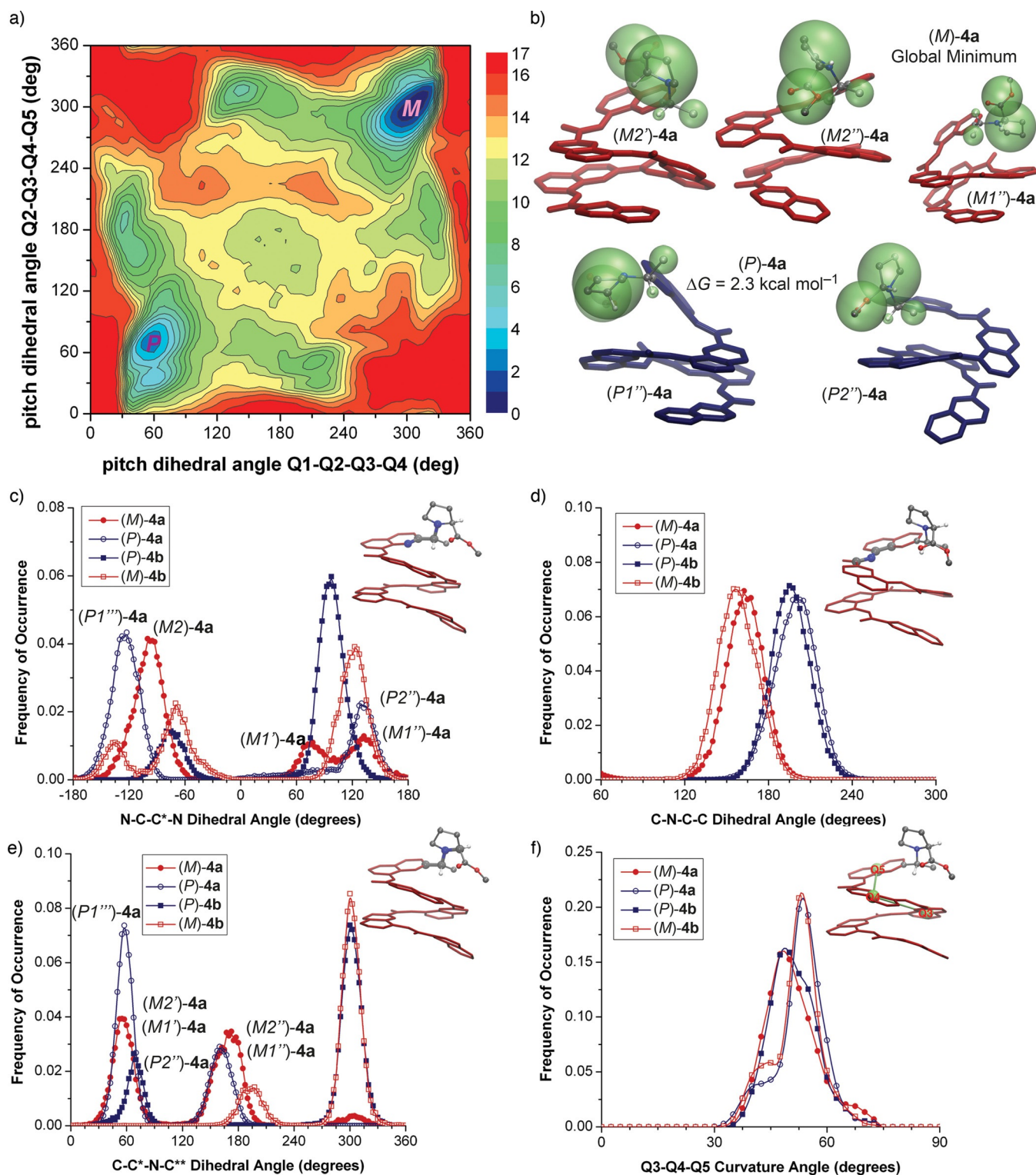


Figure 5. Free energy profile (a, energy in kcal mol⁻¹) with respect to the two pitch dihedral angles of **4a** in chloroform. Snapshots (b) of the conformations from the two helical basins (*M*)-**4a** and (*P*)-**4a**. Distributions (c–e) of backbone atomistic dihedral angles of the (*M*)-**4a**/*(P)*-**4b** and (*P*)-**4a**/*(M)*-**4b** conformations. Distribution (f) of the Q3-Q4-Q5 curvature angle of the (*M*)-**4a**/*(P)*-**4b** and (*P*)-**4a**/*(M)*-**4b** conformations. The dihedral angles and curvature angle in question are displayed in the upper-right corner of each respective distribution.

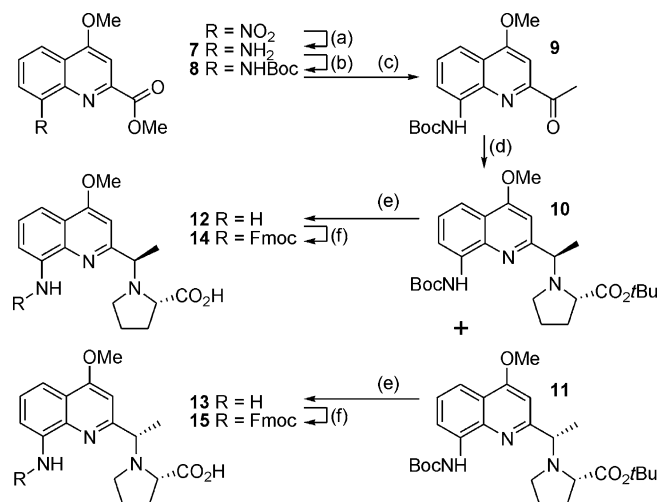
tional sampling variance between enantiomers is smaller but still visible.

In summary, the mechanism of biasing for the proline functionalized oligomers is similar to that of the morpholine-based

oligomers. One needs the right combination of C* chirality and helix handedness to appropriately arrange the three C* substituents to minimize steric repulsion. The second stereogenic center C** plays a lesser role in inducing bias.

Synthesis of proline-functionalized monomers and oligomers

In order to experimentally verify the computational results, proline-functionalized monomers and oligomers were synthesized (Scheme 1, Figure 6, Figure 7). The starting material, methyl 4-methoxy-8-nitro-quinoline-2-carboxylate was prepared as previously reported.^[7a] Its nitro group was first hydrogenated to give **7** and the resulting amine was protected with a Boc group (**8**). Compound **8** was exposed to methyl lithium to produce ketone **9** which was subjected to a reductive amination by *L*-proline *tert*-butyl ester to afford a 1:1 mixture of diastereomers **10** and **11**. Enriched samples of each diastereomer were obtained thanks to their different solubility in hexane. Further purification by reverse-phase chromatography afforded **10** and **11**, both with <0.2% diastereoisomer cross-contamination, in 30 and 28% isolated yield, respectively. Separate treatments with TFA then with Fmoc-Cl gave the corresponding Fmoc-protected acid monomers **14** and **15**. The absolute configurations of these diastereotopic monomers were determined by X-ray crystallographic analysis of **10** and **15**



Scheme 1. Synthesis of Fmoc-acid monomers **14** and **15**. Conditions: a) H₂, Pd/C, ethyl acetate, RT; b) Boc₂O, 1,4-dioxane, 100 °C; c) methyl lithium, lithium bromide, anhydrous THF, -100 °C, 2 h; d) *tert*-butyl (2*S*)-pyrrolidine-2-carboxylate, sodium cyanoborohydride, AcOH, anhydrous 1,2-dichloroethane, 60 °C; e) TFA, DCM, RT; f) Fmoc-Cl, NaHCO₃, H₂O/1,4-dioxane, 0 °C to RT, 1 day.

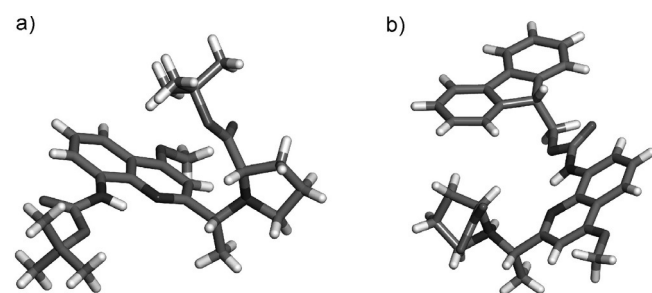


Figure 6. Crystal structures of: a) **10** and b) **15**.

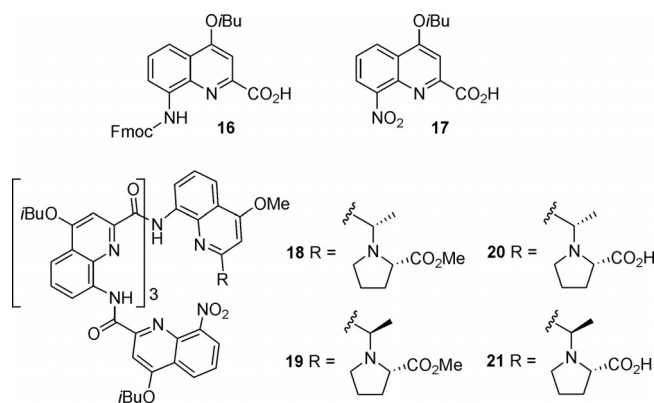


Figure 7. Structures of **16**–**21**.

(see the Supporting Information). Crystals of **10** were obtained by slow evaporation of an acetonitrile solution. Structure determination showed that the chiral center linked to the quinoline ring has an *R* configuration (Figure 6a). The HCl salt of **15** crystallized from H₂O/CH₃CN in presence of HCl (5 equiv). Structure elucidation confirmed it has the opposite stereochemistry (Figure 6b).

Proline-functionalized pentaamide oligomers **18**–**21** (Figure 7) were then prepared according to previously reported solid-phase synthesis protocols.^[21] Monomers **14** or **15** were loaded on low-loading Wang resin as C-terminal units. Sequences were elongated with monomer **16** and terminated by 8-nitro-substituted monomer **17**. Both **16** and **17** bear 4-isobutoxy chains which confer the oligomers with high solubility in chlorinated and aromatic solvents. Cleavage from the resin using TFA/DCM (50:50 v/v) afforded acids **20** and **21**, which correspond to **5 a** and **6 a**, respectively. Cleavage using MeOH/THF/DBU (49:49:2 v/v/v) yielded methyl esters **18** and **19**, which correspond to **3 a** and **4 a**, respectively.

Experimental investigation of handedness induction in proline-functionalized oligomers

Helix handedness induction was assessed by ¹H NMR spectroscopy and circular dichroism (CD) in chloroform, the solvent used for the metadynamics FEP calculations. CD permits the absolute assignment of the preferred handedness:^[17] typically, quinoline carboxamide *P* and *M* helices feature positive and negative CD bands, respectively, near 385 nm. In addition, *P* and *M* helices in solution (CDCl₃) are in slow exchange on the NMR time scale at room temperature for pentaamides and longer oligomers. When equipped with a chiral functionality, *P* and *M* helices are diastereomeric and give rise to distinct sets of signals which, by integration, allow the direct quantification of helix sense bias. The CD spectra of **18** and **19** show positive and negative CD bands at 385 nm, respectively (Figure 8e). This validates the computationally predicted helix sense preference for both compounds. The CD spectra have almost equal intensity ($\Delta\epsilon = 19$ and -18 cm²mmol⁻¹ for **18** and **19**, respectively) confirming the prediction that handedness preference is determined by the stereogenic center closest to the quinoline

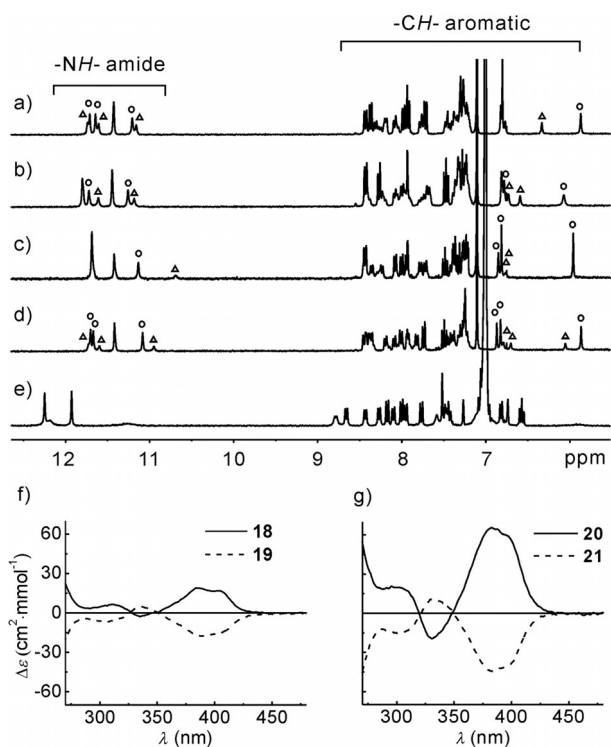


Figure 8. Excerpt of the ^1H NMR spectra at 298 K of oligomers: a) **18**, b) **19**, c) **20**, d) **21** in CDCl_3 , and e) **21** in $[\text{D}_6]\text{benzene}$ containing TFA (5 equiv). Circles and triangles indicate distinguishable major and minor species, respectively. CD spectra at 298 K of oligomers **18** (f, solid curve), **19** (f, dashed curve), **20** (g, solid curve), and **21** (g, dashed curve) in CHCl_3 .

ring, and that the proline chiral carbon has less influence. Nevertheless, CD bands appeared to be weaker than expected for a complete handedness bias in a pentaamide strand. Indeed, NMR spectroscopy showed that the ratio between major and minor helical diastereomers is only on the order of 60:40 (Figure 8a,b), a value significantly lower than predicted by the calculated FEPs.

Carboxylic acid terminated **20** and **21** showed more intense CD bands than their corresponding methyl esters, and NMR spectroscopy confirmed a stronger bias around 85:15 for the former and 75:25 for the latter (Figure 8c,d). The slightly different proportion is consistently reflected in CD intensity ($\Delta\epsilon = 65$ and $-45 \text{ cm}^2 \text{ mmol}^{-1}$ for **20** and **21**, respectively, Figure 8f) and indicates that the proline stereogenic center has some weak influence. The handedness sense is the same as for the esters and is consistent with that predicted by FEPs (Supporting information Figures S5 and S6). However, in this case, we did not endeavor to draw firm conclusions from the calculations because we could not obtain unequivocal experimental evidence that amino acids **20** and **21** were indeed under amino-acid forms in chloroform solution, without any contribution of ammonium-carboxylate zwitterionic species, or influenced by water which was not modeled in metadynamics studies. For a practical use of the C-terminal proline-based unit, for example, in the context of the recognition of a biomolecule by a helical foldamer, a complete handedness induction is desirable. We thus screened a number of other solvents and

conditions and found that helix handedness bias was close to 100% under acidic condition in apolar solvents. For example, in the ^1H NMR spectrum of **21** in $[\text{D}_6]\text{benzene}$ containing TFA (5 equiv), the minor species is hardly detectable (Figure 8e). Thus, one can envisage incubating longer oligomers in this solvent mixture in order to effectively induce handedness, and to then carry out studies in aqueous medium in which handedness will be kinetically locked.^[16]

Conclusion

We have established that metadynamics FEPs provide a reliable prediction tool of helix handedness bias in quinoline-based aromatic oligoamide helical foldamers. Calculations in an explicit solvent (chloroform) were reproducible and systematically predicted the correct handedness preferences. The extent of helix handedness bias was in some cases different from that observed experimentally. In addition, extracting conformations from the *M*- and *P*-helical basins using the metadynamics trajectories provided in each case sensible structural features to explain the observed handedness bias. Typically, we find that steric hindrance is apparent in the less favored helical diastereomers and forces the helix to deviate from its most stable conformations. In most cases, these effects would not be easy to predict by a simple observation of the structures, hence the interest of our approach. The prediction that a new C-terminal proline-functionalized monomer could bias helix handedness was experimentally validated. The outcome was the optimization of the synthesis of Fmoc-acid monomers **14** and **15**, their incorporation into oligomers, and the identification of conditions under which handedness bias is close to quantitative. We believe that the predictive power of metadynamics calculation will prove to be generally useful for a variety of existing helical aromatic backbones.^[18]

Acknowledgements

This work was supported by the China Scholarship Council (predoctoral fellowship to X.H.). We thank Dr. Brice Kauffmann for assistance with crystallography. Computational studies were supported by NSF MSN-1049771 and MRI CHE-1229564 grants.

Keywords: aromatic oligoamides · computational chemistry · foldamers · helical structures · metadynamics

[1] a) J. J. L. M. Cornelissen, A. E. Rowan, R. J. M. Nolte, N. A. J. M. Sommerdijk, *Chem. Rev.* **2001**, *101*, 4039–4070; b) E. Yashima, K. Maeda, H. Iida, Y. Furusho, K. Nagai, *Chem. Rev.* **2009**, *109*, 6102–6211.

[2] R. H. Martin, M. J. Marchant, *Tetrahedron* **1974**, *30*, 347–349.

[3] a) A. M. Abramyan, Z. Liu, V. Pophristic, *Chem. Commun.* **2016**, *52*, 669–672; b) N. Delsuc, T. Kawanami, J. Lefevre, A. Shundo, H. Ihara, M. Takafuji, I. Huc, *ChemPhysChem* **2008**, *9*, 1882–1890; c) M. M. Green, J. W. Park, T. Sato, A. Teramoto, S. Lifson, R. L. B. Selinger, J. V. Selinger, *Angew. Chem. Int. Ed.* **1999**, *38*, 3138–3154; *Angew. Chem.* **1999**, *111*, 3328–3345; d) S. Lifson, C. E. Felder, M. M. Green, *Macromolecules* **1992**, *25*, 4142–4148; e) M. Ohkita, J. M. Lehn, G. Baum, D. Fenske, *Chem. Eur. J.* **1999**, *5*, 3471–3481.

- [4] a) V. Maurizot, C. Dolain, I. Huc, *Eur. J. Org. Chem.* **2005**, 1293–1301; b) A. M. Kendhale, L. Poniman, Z. Dong, K. Laxmi-Reddy, B. Kauffmann, Y. Ferrand, I. Huc, *J. Org. Chem.* **2011**, *76*, 195–200.
- [5] a) E. Yashima, T. Matsushima, Y. Okamoto, *J. Am. Chem. Soc.* **1997**, *119*, 6345–6359; b) T. Nishimura, K. Tsuchiya, S. Ohsawa, K. Maeda, E. Yashima, Y. Nakamura, J. Nishimura, *J. Am. Chem. Soc.* **2004**, *126*, 11711–11717; c) N. Ousaka, Y. Inai, *J. Org. Chem.* **2009**, *74*, 1429–1439; d) K. Obata, C. Kabuto, M. Kira, *J. Am. Chem. Soc.* **1997**, *119*, 11345–11346; e) R. Sakai, I. Otsuka, T. Satoh, R. Kakuchi, H. Kaga, T. Kakuchi, *J. Polym. Sci. Part A* **2006**, *44*, 325–334.
- [6] a) Y. Okamoto, E. Yashima, *Angew. Chem. Int. Ed.* **1998**, *37*, 1020–1043; *Angew. Chem.* **1998**, *110*, 1072–1095; b) T. Nakano, *J. Chromatogr. A* **2001**, *906*, 205–225.
- [7] a) J. Buratto, C. Colombo, M. Stupfel, S. J. Dawson, C. Dolain, B. L. O’Estaintot, L. Fischer, T. Granier, M. Laguerre, B. Gallois, I. Huc, *Angew. Chem. Int. Ed.* **2014**, *53*, 883–887; *Angew. Chem.* **2014**, *126*, 902–906; b) H. Onouchi, T. Hasegawa, D. Kashiwagi, H. Ishiguro, K. Maeda, E. Yashima, *J. Polym. Sci. Part A* **2006**, *44*, 5039–5048.
- [8] a) J. Sola, G. A. Morris, J. Clayden, *J. Am. Chem. Soc.* **2011**, *133*, 3712–3715; b) B. A. F. Le Bailly, L. Byrne, J. Clayden, *Angew. Chem. Int. Ed.* **2016**, *55*, 2132–2136; *Angew. Chem.* **2016**, *128*, 2172–2176; c) J. Clayden, A. Castellanos, J. Sola, G. A. Morris, *Angew. Chem. Int. Ed.* **2009**, *48*, 5962–5965; *Angew. Chem.* **2009**, *121*, 6076–6079.
- [9] a) K. Maeda, M. Ishikawa, E. Yashima, *J. Am. Chem. Soc.* **2004**, *126*, 15161–15166; b) H. Ito, Y. Furusho, T. Hasegawa, E. Yashima, *J. Am. Chem. Soc.* **2008**, *130*, 14008–14015; c) N. Delsuc, S. Massip, J.-M. Léger, B. Kauffmann, I. Huc, *J. Am. Chem. Soc.* **2011**, *133*, 3165–3172; d) C. Tsiamantas, X. de Hatten, C. Douat, B. Kauffmann, V. Maurizot, H. Ihara, M. Takafuji, N. Metzler-Nolte, I. Huc, *Angew. Chem. Int. Ed.* **2016**, *55*, 6848–6852; *Angew. Chem.* **2016**, *128*, 6962–6966.
- [10] a) E. Yashima, K. Maeda, Y. Okamoto, *Nature* **1999**, *399*, 449–451; b) K. Shimomura, T. Ikai, S. Kanoh, E. Yashima, K. Maeda, *Nat. Chem.* **2014**, *6*, 429–434.
- [11] a) Y. Inai, Y. Kurokawa, T. Hirabayashi, *Biopolymers* **1999**, *49*, 551–564; b) Y. Inai, H. Komori, *Biomacromolecules* **2004**, *5*, 1231–1240; c) M. De Poli, M. D. Zotti, J. Raftery, J. A. Aguilar, G. A. Morris, J. Clayden, *J. Org. Chem.* **2013**, *78*, 2248–2255; d) R. A. Brown, T. Marcelli, M. D. Poli, J. Sola, J. Clayden, *Angew. Chem. Int. Ed.* **2012**, *51*, 1395–1399; *Angew. Chem.* **2012**, *124*, 1424–1428.
- [12] a) H. Jiang, J.-M. Leger, I. Huc, *J. Am. Chem. Soc.* **2003**, *125*, 3448–3449; b) T. Qi, V. Maurizot, H. Noguchi, T. Charoenraks, B. Kauffmann, M. Takafuji, H. Ihara, I. Huc, *Chem. Commun.* **2012**, *48*, 6337–6339.
- [13] A. Laio, M. Parrinello, *Proc. Natl. Acad. Sci. USA* **2002**, *99*, 12562–12566.
- [14] a) P. S. Shirude, E. R. Gillies, S. Ladame, F. Godde, K. Shin-ya, I. Huc, S. Balasubramanian, *J. Am. Chem. Soc.* **2007**, *129*, 11890–11891; b) L. Delaurière, Z. Dong, K. Laxmi-Reddy, F. Godde, J.-J. Toulmé, I. Huc, *Angew. Chem. Int. Ed.* **2012**, *51*, 473–477; *Angew. Chem.* **2012**, *124*, 488–492; c) S. Müller, K. Laxmi-Reddy, P. V. Jena, B. Baptiste, Z. Dong, F. Godde, T. Ha, R. Rodriguez, S. Balasubramanian, I. Huc, *ChemBioChem* **2014**, *15*, 2563–2570; d) P. K. Mandal, B. Baptiste, B. Langlois d’Estaintot, B. Kauffmann, I. Huc, *ChemBioChem* **2016**, *17*, 1911–914.
- [15] M. Jewginski, L. Fischer, C. Colombo, I. Huc, C. D. Mackereth, *ChemBioChem* **2016**, *17*, 727–736.
- [16] S. J. Dawson, A. Meszaros, L. Petho, C. Colombo, M. Csekei, A. Kotschy, I. Huc, *Eur. J. Org. Chem.* **2014**, 4265–4275.
- [17] C. Dolain, H. Jiang, J.-M. Léger, P. Guionneau, I. Huc, *J. Am. Chem. Soc.* **2005**, *127*, 12943–12951.
- [18] a) R. B. Prince, L. Brunsveld, E. W. Meijer, J. S. Moore, *Angew. Chem. Int. Ed.* **2000**, *39*, 228–230; *Angew. Chem.* **2000**, *112*, 234–236; b) M. S. Gin, J. S. Moore, *Org. Lett.* **2000**, *2*, 135–138; c) J.-L. Hou, H.-P. Yi, X.-B. Shao, C. Li, Z.-Q. Wu, X.-K. Jiang, L.-Z. Wu, C.-H. Tung, Z.-T. Li, *Angew. Chem. Int. Ed.* **2006**, *45*, 796–800; *Angew. Chem.* **2006**, *118*, 810–814; d) M. Inouye, M. Waki, H. Abe, *J. Am. Chem. Soc.* **2004**, *126*, 2022–2027; e) E. D. King, P. Tao, T. T. Sanan, C. M. Hadad, J. R. Parquette, *Org. Lett.* **2008**, *10*, 1671–1674; f) J. Zhu, Z. Dong, S. Lei, L. Cao, B. Yang, W. Li, Y. Zhang, J. Liu, J. Shen, *Angew. Chem. Int. Ed.* **2015**, *54*, 3097–3101; *Angew. Chem.* **2015**, *127*, 3140–3144; g) H.-Y. Hu, J.-F. Xiang, Y. Yang, C.-F. Chen, *Org. Lett.* **2008**, *10*, 1275–1278; h) C. Li, G.-T. Wang, H.-P. Yi, X.-K. Jiang, Z.-T. Li, R.-X. Wang, *Org. Lett.* **2007**, *9*, 1797–1800; i) Q. Gan, F. Li, G. Li, B. Kauffmann, J. Xiang, I. Huc, H. Jiang, *Chem. Commun.* **2010**, *46*, 297–299; j) J.-m. Suk, D. A. Kim, K.-S. Jeong, *Org. Lett.* **2012**, *14*, 5018–5021; k) D. A. Kim, P. Kang, M.-G. Chi, K.-S. Jeong, *Chem. Commun.* **2013**, *49*, 9743–9745.
- [19] a) Z. Liu, A. M. Abramyan, V. Pophristic, *New J. Chem.* **2015**, *39*, 3229–3240; b) A. M. Abramyan, Z. Liu, V. Pophristic, *Phys. Chem. Chem. Phys.* **2014**, *16*, 20406.
- [20] Once morpholine is protonated, the experimental bias goes up to >99% which is useful for practical applications. However, calculations have not been carried out on the protonated form.
- [21] a) B. Baptiste, C. Douat-Casassus, K. Laxmi-Reddy, F. Godde, I. Huc, *J. Org. Chem.* **2010**, *75*, 7175–7185; b) S. J. Dawson, X. Hu, S. Claerhout, I. Huc, *Methods Enzymol.* **2016**, *580*, 279–301.

Manuscript received: October 31, 2016

Accepted Article published: December 9, 2016

Final Article published: January 16, 2017